

OPENFOAM SIMULATION OF DUAL IN-LINE WIND TURBINES BASED ON ACTUATOR LINE MODEL

Huseyin Can Onel* and Ismail H. Tuncer†
Middle East Technical University
Ankara, Turkey

ABSTRACT

This study presents preliminary results of a Master's Thesis on modeling of wind turbines and wake structures using Actuator Line Model (ALM). The model adopts a computationally less expensive approach on simulating wake interactions in a wind farm with many turbines, by solving full Navier-Stokes equations and avoiding the need of boundary layer resolution over blade surfaces. Results of a single wind turbine simulation are compared to Blade Element Momentum (BEM) solutions, which is still a widely used and accepted rotor simulating method. In a second case, two turbines in tandem position are simulated and power loss in the downstream turbine is calculated. Some of the parameters which are found to be important in usage of the method are discussed. Results are presented and found to be in close agreement with BEM solutions.

INTRODUCTION

As the energy demand keeps increasing with growing human population, renewable sources gain prominence with their economical and environmental advantages. In recent years, wind has been shining out as the most harvested renewable energy resource with worldwide power capacity reaching 600 GW in 2018.

Wind farms are composed of many turbines working simultaneously under constantly changing atmospheric conditions. Good power production estimation is crucial in both operation and design stages in wind farms. Wind speed and direction are the two most important parameters affecting production of a wind farm in the broadest sense. In a smaller scale, the zone behind each turbine, where velocity is reduced and turbulence is increased due to energy extraction by the rotor, affects downwind turbines negatively. This zone is called *wake* and turbine-to-turbine wake interactions are found to be responsible of about 20% power loss compared to a wake-free scenario. However, since wake is an inevitable result of energy extraction by the turbines from the wind, minimization of its effect rises as one of the primary farm design concerns.

Regarding the aerodynamics of wind farm design, there are two main stages:

- Rotor Modeling (Turbine Design): Wind turbines are designed and optimized mostly for ideal conditions, where inflow velocity is uniform and in axial direction. Classical approaches are

*GRA in Department of Aerospace Engineering, Email: canon@metu.edu.tr

†Professor in Department of Aerospace Engineering, Email: ismail.h.tuncer@ae.metu.edu.tr

still heavily relied on in turbine design; potential flow, 2D airfoil theory and Blade Element-Momentum calculations.

- Wake Modeling (Layout Design): Turbine layout planning is done in two main scales: Choice of geographical location is called macro-siting and statistical meteorological data is heavily used, whereas coordinates of each turbine are decided in micro-siting stage where analytical and empirical simplifications are still widely used.

To calculate the power production of each turbine in the field, local flow field in the vicinity of each blade needs to be calculated accurately. Most of the turbines in a wind farm is under the influence of wake generated by upwind turbines, hence, wake structures has to be simulated accurately. Advancements in computer technologies has enabled Computational Fluid Dynamics (CFD) to go mainstream for such simulations. Today, resolving the flow around a wing in the length scale of boundary layer thickness is a common practice. However, when the length and time scales in a complete wind farm is considered, it would be seen that they fall in a very large range: extending from millimeters (in boundary layer) to kilometers (in field dimensions). Resolving this whole range becomes problematic especially when one runs a simulation with tens of turbines in a wind farm.

One of the ideas in tackling this problem is to avoid resolving the boundary layer on blade surfaces in an attempt to reduce grid size. Actuator models were emanated from this idea. One of the most recent and highest fidelity models is the so called Actuator Line Model (ALM), first introduced by Sorensen and Shen [2002]. In ALM, blades are represented as virtual "lines" which are divided into elements as in the Blade Element-Momentum approach. Instead of calculating 3D pressure distribution over blade surfaces to find torque and thrust, these forces are calculated for each element by use of 2D airfoil theory and passed into the flow field.

In this study, a model wind turbine is modeled with ALM and various simulations with single and multiple wind turbines are carried out. Blade loadings, wake profiles and performance parameters are calculated and compared to other studies. Although ALM saves computational cost, there is a certain level of drop in accuracy. The trade-off between physical accuracy and computational profitability of ALM is examined. Some important simulation parameters and the model's sensitivity is discussed.

METHOD

In this study, CFD simulations of a model wind turbine are performed, findings are compared to results obtained by other methods and presented by other studies. Incompressible and unsteady Navier-Stokes equations are discretized to obtain time-accurate numerical solutions. Spatial discretization (generation of the grid) and solution are done by open source flow solver OpenFOAM modules (Weller et.al. [1998]). Turbine blades are introduced into the solution domain using ALM to save on computational cost. ALM implementation is done by the OpenFOAM library extension turbinesFoam (Bachant [2016]). 2D airfoil calculations are done by low Reynolds Number airfoil analysis code XFOIL (Drela [1988]). BEM results are often used as reference for validation and verification, the open source BEM code QBlade is used for solutions (Marten et.al. [2013]).

Flow Solver: OpenFOAM

OpenFOAM is an open source toolbox which includes flow solvers suitable for various flow cases, as well as a basic level grid generator. Features can be added or modified in OpenFOAM according to the need. It uses finite volume approach for discretization of partial differential equations and also can run in parallel. OpenFOAM's transient flow solver for incompressible fluids, pimpleFoam, is used in this study for simulations. pimpleFoam derives its name from the combination of PISO (*Pressure Implicit with Splitting of Operator*) and SIMPLE (*Semi-Implicit Method for Pressure-Linked Equations*) algorithms. Incompressible fluid assumption is made due to the fact that the highest velocity magnitude in simulations (which is the linear tip speed of blades) does not exceed

$M = 0.3$. The Navier-Stokes equations governing the fluid flow is given by:

$$\nabla \cdot \vec{u} = 0 \quad (1)$$

$$\frac{\partial \vec{u}}{\partial t} + \nabla \cdot (\vec{u}\vec{u}) = -\nabla p + \nabla \cdot (\nu \nabla \vec{u}) + \vec{f} \quad (2)$$

where \vec{u} : velocity vector, p : pressure per density, ν : kinematic viscosity and f is the body force per density per volume. Turbulence is modeled using Large Eddy Simulation (LES) approach, in which large-scale eddies are resolved by applying a low-pass filter to Navier-Stokes equations, yielding:

$$\widetilde{\nabla \cdot \vec{u}} = 0 \quad (3)$$

$$\frac{\partial \widetilde{\vec{u}}}{\partial t} + \widetilde{\vec{u} \nabla \vec{u}} = -\nabla \widetilde{p} + \nu \nabla^2 \widetilde{\vec{u}} - \nabla \cdot \tau^d + \widetilde{f}_b \quad (4)$$

$$\tau_{ij}^d = \tau_{ij} - \frac{1}{3} \delta_{ij} \tau_{kk} \quad (5)$$

where curly over-bar symbol represents filtered quantities. Here, τ_{ij}^d is the remaining deviatoric component of the SGS stress tensor. To obtain closure, it is expressed in terms of filtered velocity $\widetilde{\vec{u}}$ and pressure \widetilde{p} . This is achieved by using the Smagorinsky model (Smagorinsky [1963]):

$$\tau_{ij}^d = -2\nu_{SGS} S_{ij} \quad (6)$$

$$\nu_{SGS} = (C_S \Delta)^2 |S| \quad (7)$$

$$S = \frac{1}{2} (\widetilde{u}_{j,i} + \widetilde{u}_{i,j}) \quad (8)$$

$$|S| = (2S_{ij} S_{ij})^{(1/2)} \quad (9)$$

where ν_{SGS} is the sub-grid scale viscosity, S is the rate of strain tensor and C_S is the model constant. Δ is taken as the cube root of cell dimensions in all directions, i.e. $\Delta = (\Delta_x \Delta_y \Delta_z)^{(1/3)}$. In simulations where turbulence is dominantly isotropic, suggested C_S value is 0.168.

Actuator Line Model

Conventionally, blades are introduced into the flow domain as solid boundaries and boundary conditions are applied. Then, pressure distribution over the surfaces are calculated either by the use of wall functions or fully resolving the boundary layer. Rotational movement of the rotor is usually obtained by Multiple Reference Frames (MRF) or Sliding Mesh Interface (SMI) methodologies. Although this approach has been validated in numerous studies, it requires a very large number of cells in blade vicinity. This need becomes problematic when many turbines are required to be simulated simultaneously, i.e. a wind farm.

In the simplest sense, Actuator Line Model (ALM) (Sorensen and Shen [2002]), suggests dividing blades into a finite number of segments (much like the case in BEM) and calculating lift and drag forces by use of 2D airfoil theory; thus making boundary layer resolution avoidable. This force is then passed into cell centers as an additional body force term in the momentum equation (through f term as in momentum equation in Eq. 2). Lift and drag coefficient data of airfoil profiles are calculated and tabulated with respect to angle of attack and Reynolds numbers prior to the simulations using XFOIL (Drela [1988]). This readily available data is then used during simulations in lift and drag equations, given as $L = 0.5\rho U_{rel}^2 c_l c_s$ and $D = 0.5\rho U_{rel}^2 c_d c_s$, respectively. These forces are calculated for each blade element at every time step and are acted on the actuator points, which corresponds to the quarter chord at the mid span location of elements. In contrary to the BEM, where iterations are done on axial and tangential induction factor; calculated force and resultant velocity field are iterated on in a coupled fashion in ALM. Resultant forces are also distributed along neighboring cells

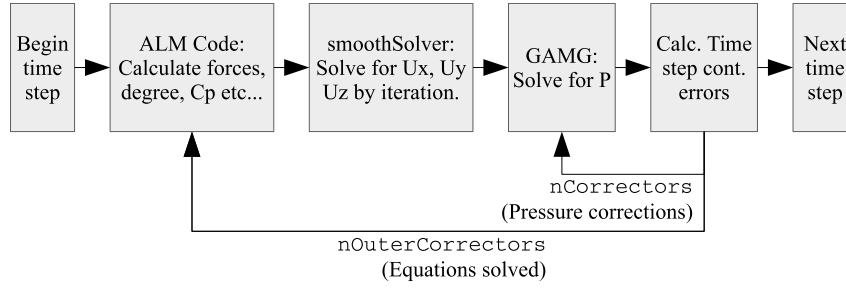


Figure 1: Flow chart showing the PIMPLE loop within a single time step

instead of being imposed on the closest cell center only, in an attempt to prevent singular behavior and instability.

Velocity Sampling and Force Projection: Application of the Actuator Line Model involves two steps which have crucial effect on the results and poses questions whose answers are still uncertain to this day:

- Velocity sampling: how and where to monitor the velocity vectors that are going to be used in angle of attack and incoming flow speed estimations? This is crucial in finding c_l and c_d accurately, so that force computation is also accurate.
- Force projection: how to distribute the computed forces among the neighboring cells, so that an accurate pressure field can be obtained that acceptably resembles the real pressure distribution over blade surfaces.

Several approaches to these problems exist in the literature. A simple yet well-performing method for velocity sampling is to use the velocity vector at the actuator point (mid-span of the element, at the quarter chord point) by interpolation. Force distribution is often done in the form of a 3D Gaussian distribution function for each blade element, given as:

$$\eta = \frac{1}{\epsilon^3 \pi^{3/2}} \exp\left(-\left(\frac{|\vec{r}|}{\epsilon}\right)^2\right) \quad (10)$$

Width of the projection sphere remains an ambiguous parameter, which is discussed in the single wind turbine simulation case in the results section.

Tip Loss Correction: Since the blades are not physically present in the solution domain, the "pressure leakage" towards blade tips can not be captured accurately in this model. Hence, it is modeled in a similar fashion with BEM methodology. The tip correction factor based on Glauert's suggestion and further improved by Shen et.al. is used in this study (Shen et.al. [2005]);

$$F_{loss} = \frac{2}{\pi} \cos^{-1}\left(\exp\left(-g \frac{N_B(R-r)}{2r \sin \phi}\right)\right) \quad (11)$$

where g is given as;

$$g = \exp(-0.125(N_B \lambda - 21)) + 0.1 \quad (12)$$

and constants are acquired from measurements.

Solution Grid

Solution domain is discretized into a structured mesh where cell size starts at the coarsest on free stream and is gradually refined towards the rotor plane. Rotor center is located at $(0, 0, 0)$. side boundaries are set to slip condition in the uniform flow case, since the boundary effects are absent.

Cell size at the outer boundaries is $63m$, which is refined towards the rotor area level by level, finally reaching approximately $1m$ to $4m$ in the actuator line vicinity (depending on the grid size under consideration). The atmospheric boundary layer (ABL) flow case differs only at the ground boundary, which is located at $z = -90m$ plane.

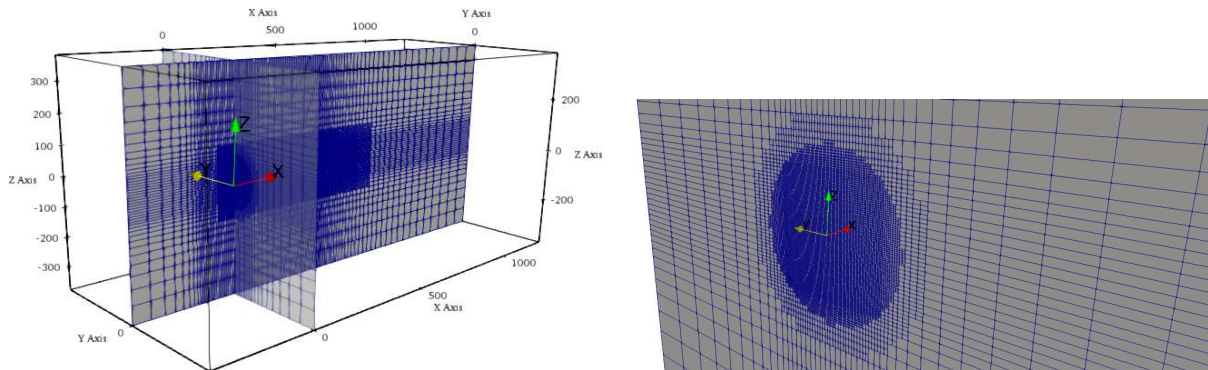


Figure 2: 3D view of the mesh on x and y mid plane sections (left) and rotor region zoomed (right)

Domain extends are $-3D$ to $3D$ in lateral (y and z) directions and $-3D$ to $10D$ in flow (x) direction. Grid size changes with the refinement level at the rotor plane, which varies between $\Delta_g/R = 1/16$ and $1/64$, typically in the range of $0.4M - 4.7M$ cells. OpenFOAM's built-in blockMesh and snappyHexMesh utilities were used for grid generation.

Blade Element Momentum Theory

Generalized Momentum Theory provides an insight for a theoretical disk with optimal induction factors but does not involve characteristics of the turbine; such as blade geometry (twist and taper), number of blades and airfoil properties. Developed by Glauert in 1935, BEM is a simple yet powerful approach to model a rotor, which is still widely in use today. ALM inherits its main concept from BEM, hence it provides comparable results to verify ALM solutions. Results in this study are often compared against BEM solutions, which are obtained by QBlade, an open source BEM solver developed by Marten et.al. Marten et.al. [2013].

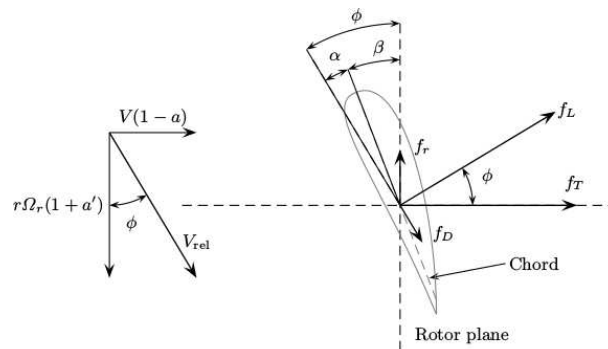


Figure 3: Relative velocity, angle definitions and forces acting on a blade section. (Source: Bianchi et.al. [2007]) Used both in BEM and ALM.

RESULTS AND DISCUSSION

NREL's 5MW reference wind turbine (Jonkman et.al. [2009]) is used as the sample turbine and it is modeled using Actuator Line Model (ALM). The NREL 5MW HAWT is 126m in diameter, has 3 blades and rated at $U_\infty = 11.4m/s$ and $TSR = 7$ (corresponding to $\approx 12.1RPM$). Power and thrust coefficients are given as $C_P = P/(0.5\rho U_\infty^3 A_d)$ and $C_T = T/(0.5\rho U_\infty^2 A_d)$ respectively (where A_d is the area swept by blades). The model is tested for 2 main cases:

1. Single Turbine Case, where blade loadings and performance of a single turbine is examined by imitating Blade Element Momentum (BEM) conditions.
2. Two Turbines in Tandem Position, where the power loss of a turbine under the influence of wake generated by another turbine is observed in a back-to-back configuration of two turbines.

Single Turbine Case

In this case, a single turbine is placed in a domain isolated from boundary effects to satisfy similar conditions with BEM method. Flow is axial and downstream distance is kept long enough to prevent wake reflections. NREL5MW wind turbine is operated at its rated conditions, i.e. $U_\infty = 11.4m/s$ and $TSR = 7$.

As stated in the Method section, force projection width is one of the most important simulation parameters in Actuator Line Model. Since chord based and cell size based methods are the two mostly used approaches in the literature, they are experimented with in this section. Cell size based ϵ approach goes along with the grid size, hence, a grid independence study has been conducted on three different grid refinement levels of $\Delta_g/R = 1/16, 1/32$ and $1/64$, namely coarse, medium and fine, respectively. Also, two different constant projection width values are tested in an attempt to observe the effect of ϵ (Figure 4).

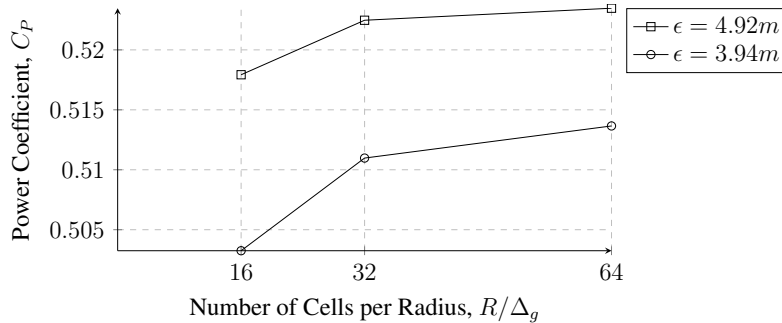


Figure 4: Convergence of power coefficient C_P with grid size at rotor plane for different ϵ values.

It should be noted that another simulation parameters that plays an important role is the time step size, evaluated in terms of how many cells does the blade tip travels in a single time step. In the literature, it is often suggested that movement of the blade tip should not exceed 1 cell size. Accordingly, blade tip travel is set to $0.9\Delta_g$ in this section. Using these settings, grid convergence can be seen on Figure 4, where the power coefficient of the turbine is used as the convergence criteria. A significant difference is observed between $\Delta_g/R = 1/16$ and $\Delta_g/R = 1/32$, then a converging trend is visible towards $\Delta_g/R = 1/64$. ϵ also affects the power prediction; as the force is projected onto a larger volume, estimated power also increases.

Power coefficient of the turbine gives an idea about the accuracy of the model in a broad sense. For a better evaluation of the model's performance, distributions of angle of attack α and tangential force F_t along blades are also examined. These two parameters have been chosen for evaluation because of the fact that α is the primary parameter in determination of c_l and c_l and F_t is the force that generates the torque (and hence the power).

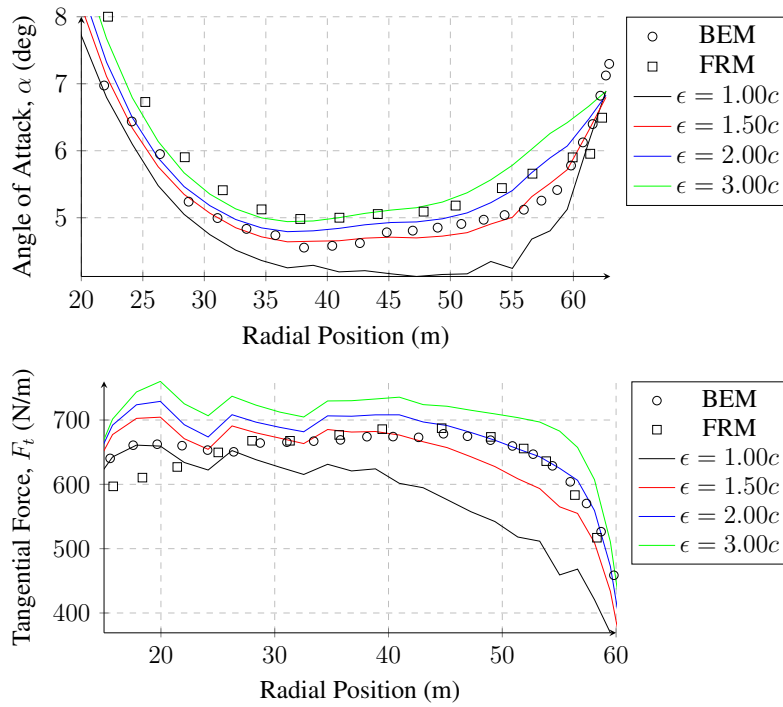


Figure 5: Computed α (top) and F_t (bottom) for different chord based ϵ values ($\Delta_g/R = 1/32$) (FRM: Dose et.al. [2018])

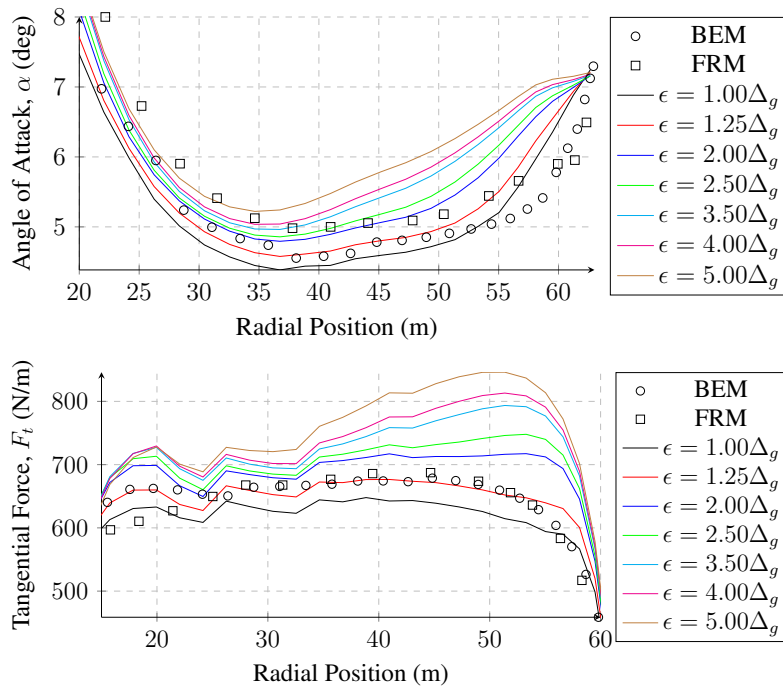


Figure 6: Computed α (top) and F_t (bottom) for different cell size based ϵ values ($\Delta_g/R = 1/32$) (FRM: Dose et.al. [2018])

Results for chord based and cell size based ϵ can be seen on Figures 5 and 6, respectively. Using a chord based ϵ , best agreement with both BEM and Fully Resolved Mesh (FRM) results is achieved with $\epsilon = 2.0c$, even though a significant discrepancy is visible towards the root. Chord based projection width approach falls short in capturing an overall fitting curve. This is pronounced when the behavior of the computed F_t varies with changing chord multiplier; variation towards the tip is significantly larger than the root vicinity. On the other hand, cell size based ϵ approach yields a better agreement with BEM overall, especially with $\epsilon = 1.25\Delta_g$. Similar to the chord based approach, variation in projection width causes different behavior in α and F_t curves at root and tip vicinity also in cell size ϵ . Nevertheless, thanks to its better overall fit with BEM results, cell size based ϵ is used for the rest of this study. Since $\Delta_g/R = 1/32$ grid refinement level yields the best accuracy/computational cost balance, it is used along with $\epsilon = 1.25\Delta_g$.

Results at Various Rotational Speeds:

In a real-life operating wind farm, turbines are subject to significant variations of wind speed. Although turbines are designed for a certain wind speed and corresponding rotational speed (rated conditions), they often require to operate in off-design conditions. Thus, the Actuator Line Model should yield reliable results in such situations. To test the model's capability at various tip speed ratios (rotational speeds) simulations are performed for $TSR = 2 - 12$ at constant $U_\infty = 11.4m/s$ and results are compared with BEM.

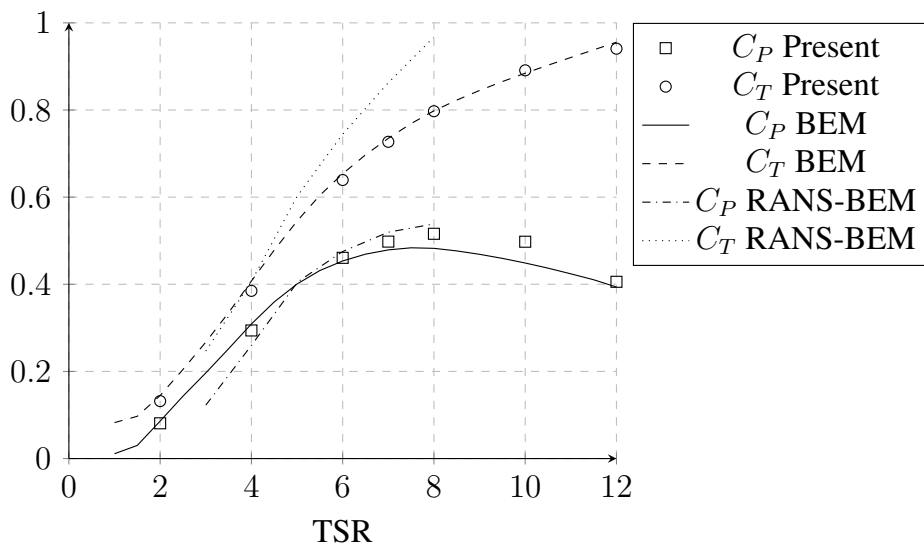


Figure 7: Computed power and thrust coefficients for different tip speed ratios (at $U_{ref} = 11.4m/s$) (RANS-BEM: Burmester et.al. [2016])

Power coefficient C_P and thrust coefficient C_T versus TSR curves are in close agreement with BEM results. A significant difference is observed between $TSR = 7 - 10$, which might be related to the stall conditions at certain blade sections, which are poorly reflected in c_l and c_d data (Figure 7). The discrepancy against RANS-BEM results are attributed to the difference of c_l and c_d data, originating from the different methods used (2D integral boundary layer theory and RANS solutions). In terms of angle of attack and tangential force distributions, results are very close to BEM solution, especially when TSR is close to the rated condition of $TSR = 7$ (Figure 8). At higher and lower TSR conditions, computed distributions are also found to be acceptably close to BEM results, despite the slight inconsistency at small and large radial positions.

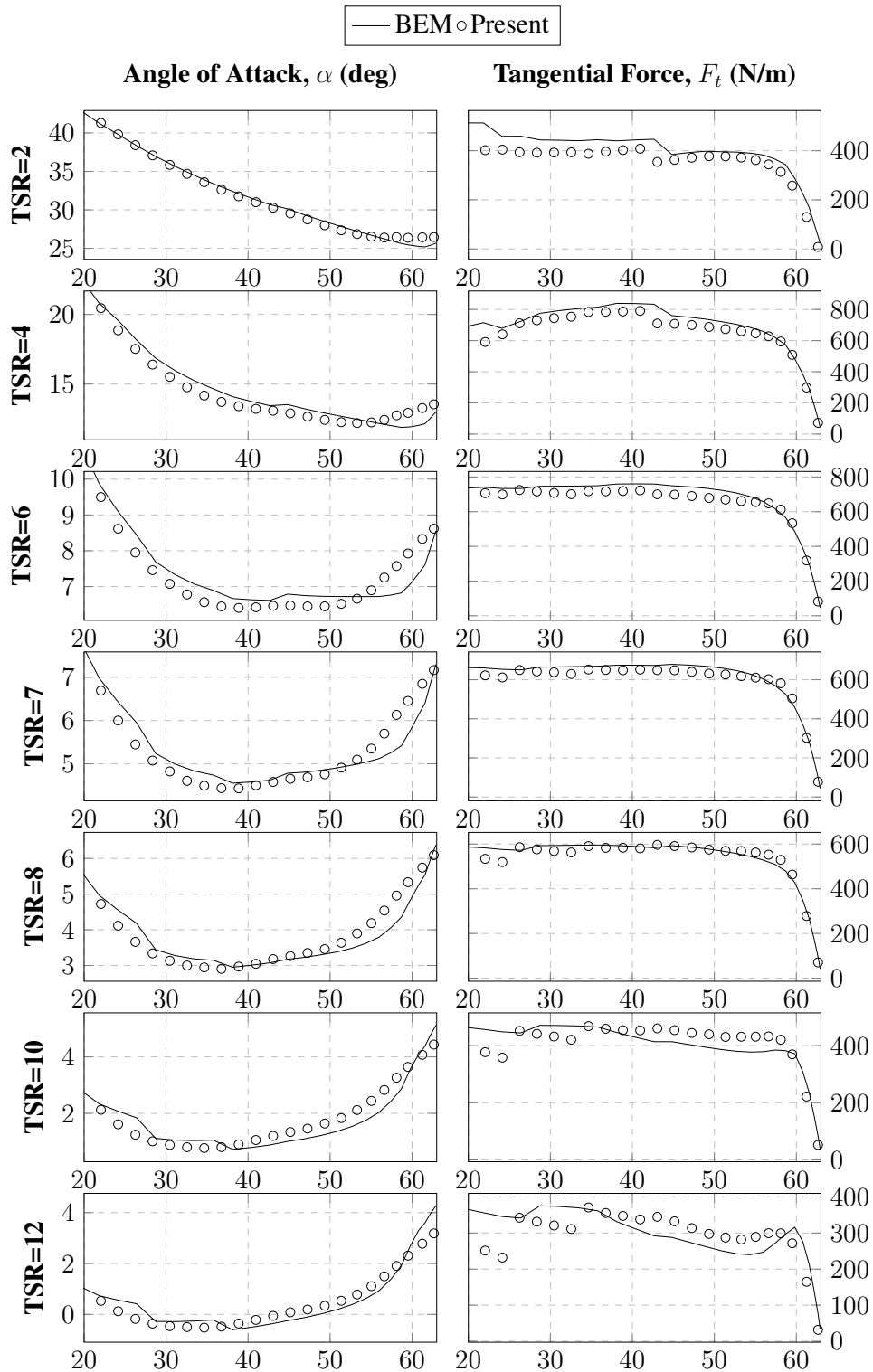


Figure 8: Computed α and F_t distributions for different TSR values ($U_{ref} = 11.4m/s, \Delta_g/R = 1/32$)

Dual Turbines in Tandem

Using the best performing force projection width parameter $\epsilon = 1.25\Delta_g$ found in the previous section, two axially aligned NREL5MW rotors operating at identical conditions are simulated and wake interactions are examined. Instead of the rated conditions, both rotors are operated at $TSR = 7.3$ at $U_\infty = 8.0m/s$. Distance between rotors are set to $7D = 882m$ and the flow is simulated for $t_{max} = 500s$.

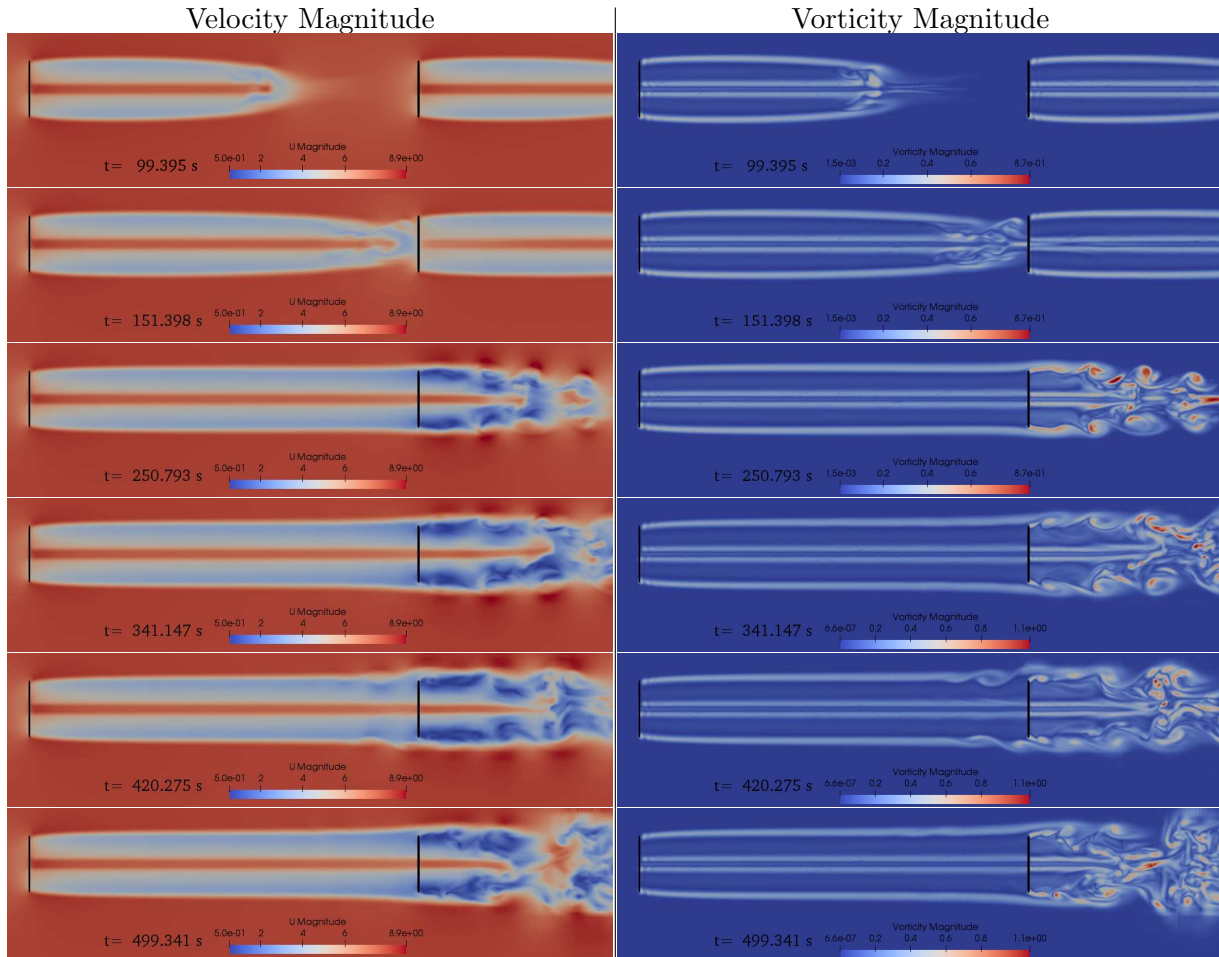


Figure 9: Velocity and vorticity magnitude contours during wake development (mid-z-plane section)

Instantaneous axial velocity contours on the mid-z-plane section shows the distinct velocity deficit in the wake zone, extending from WT1 to WT2 (Figure 9). It takes approximately 150s for wake generated by WT1 to reach the downstream turbine. Up to that point, wake of WT2 is identical to that of WT1. Upon initial impingement of the wake, vortex zones with high magnitudes are observable just behind WT2, which are then turn into a more homogeneous structure and reach a periodically-steady state.

Non-dimensional velocity deficit curves along y-axis at different x-stations reveals how wake zone develops more clearly (Figure 10). Velocity deficit reaches its maximum at $x = 1D$ and slowly spreads as it moves downstream. Although diffusion is very small, axial speed increases slightly at $x = 6D$. Past WT2, due to the additional energy extraction by the downstream rotor, velocity deficit reaches its maximum after WT2. It can be seen that the vortex breakdown is more rapid in the wake region of WT2 compared to that of WT1. This is attributed to the additional turbulent energy conveyed into the wake by WT2, which increases the rate of diffusion of momentum.

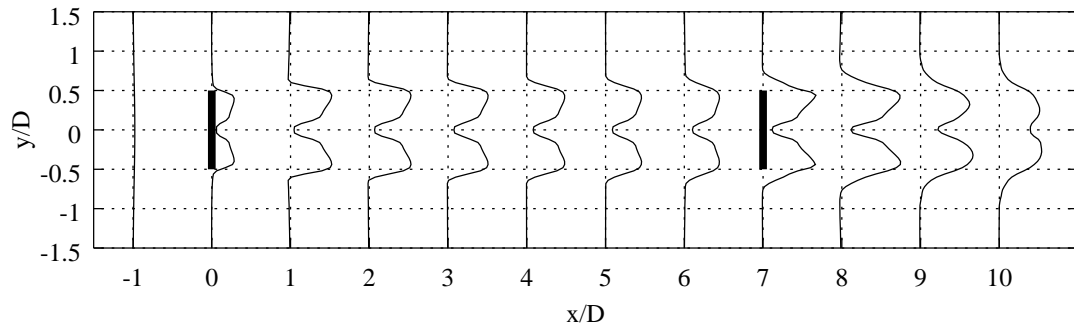


Figure 10: Mean axial velocity deficit ($1 - U_x/U_{ref}$) profiles along y (horizontal) axis at different x stations

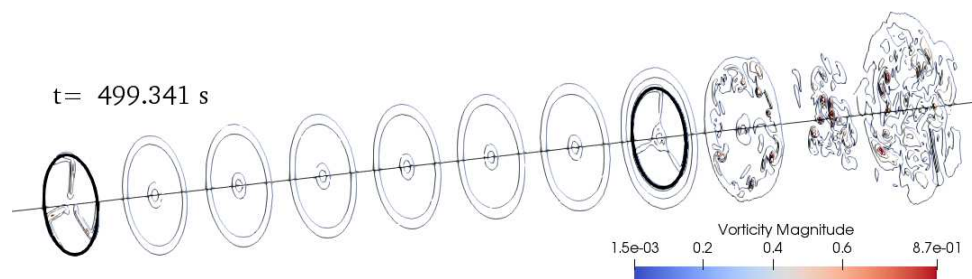


Figure 11: Vorticity contours at various x -station planes

Vortex magnitude contours at various x -stations also shows a similar trend (Figure 11). Vortices shed from blade tips form a tubular structure, which extends from upstream rotor to downstream rotor while keeping its shape almost intact. As the wake goes through WT2, due to the increased eddy motion, vortex contours exhibit a more dispersed shape. This can also be seen in 3D vortex and Q -criterion iso-surface plots (Figures 12 and 13, respectively). The main difference in Q -criterion iso-surfaces is the absence of structures originating from the blade tips and new structures showing up in the root region. This is attributed to the definition of Q value, which includes the strain rate tensor in addition to the vorticity magnitude as a diminishing term. This means that rate of strain is high in the blade tip region, whereas low in the root region of the wake zone.

The power coefficient C_P histogram of upstream (WT1) and downstream (WT2) turbines shows how the computed power changes with time (Figure 14). Computed power is identical and over-estimated for both turbines up to $t = 100s$, due to the unsteady flow characteristics originating from the instantaneous introduction of the rotors into the flow domain of uniform flow. Power of WT2 starts decreasing slightly after $t = 100s$ where the effect of wake begins to be felt by WT2. After $t = 150s$, an erratic C_P graph can be seen. This is the transitional point, where the starting vortex generated by WT1 impinges on WT2. This continues up to $t \approx 230s$. After that point, power production of WT2 goes into a periodically-steady state with a certain cyclic behavior.

Power loss in the second wind turbine is estimated as 86% in this simulation, which is extremely high compared to the real-life instances. Nevertheless, this value is in very close agreement with what

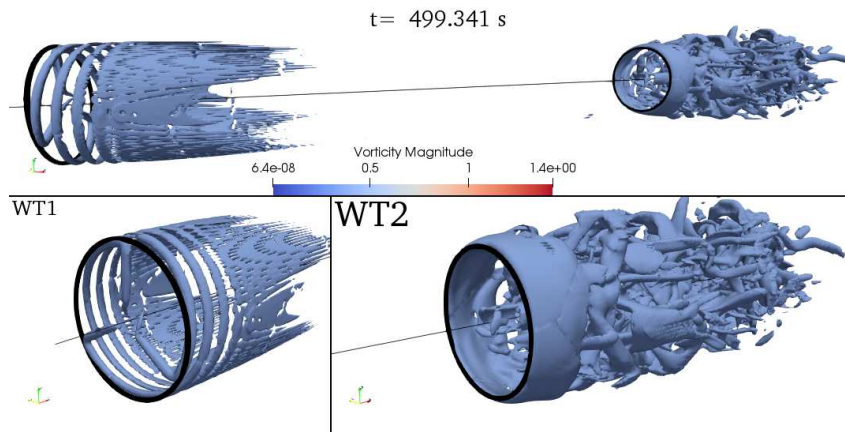


Figure 12: Vorticity $\zeta = 0.38$ iso-surfaces

was found by Schmitz and Jha (Schmitz and Jha [2013]) in identical conditions. This outcome is attributed to the lack of atmospheric turbulence in simulations, which is primarily responsible for the break-down of the wake and diffusion of the velocity deficit. Schmitz and Jha also mentioned the fact that tip speed ratio of WT2 is not adjusted according to the low-speed incoming air, which would be the case in a real-life operation in an attempt to increase the power output of the wind turbine.

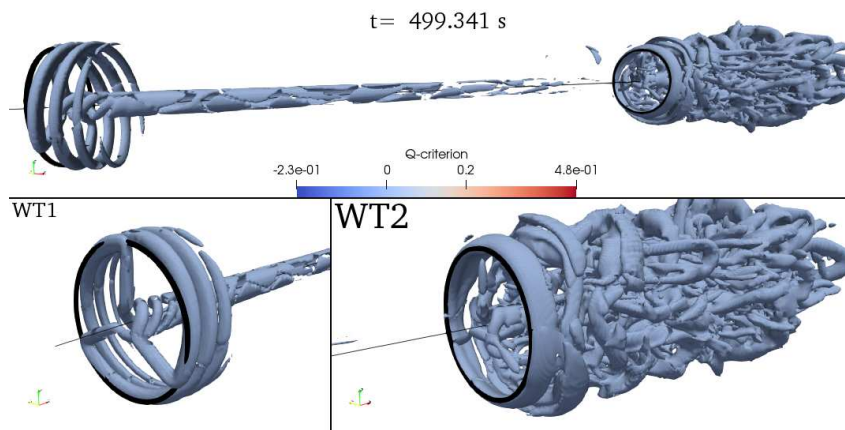


Figure 13: Q-criterion $Q=0.005$ iso-surfaces

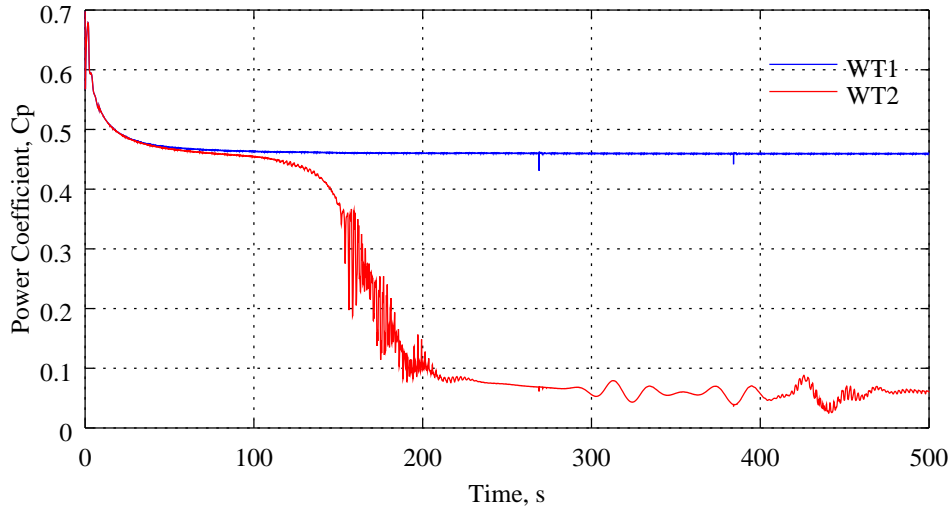


Figure 14: Power coefficient C_P histogram of upstream and downstream wind turbines in tandem configuration (at $U_{ref} = 8.0m/s$)

CONCLUSION

An NREL5MW wind turbine rotor is modeled with Actuator Line Model and the flow around it is solved using OpenFOAM and LES turbulence model. In a single and isolated rotor case, one of the critical simulation parameters of the model, force projection width, is experimented with. On a solution grid with $\Delta_g/R = 1/32$ refinement level, the force projection width control parameter $\epsilon = 1.25\Delta_g$ has yielded the best agreement with BEM results. Other than the rated conditions, the model has performed well at lower and higher tip speed ratios. Using this setting, two axially aligned wind turbines in tandem configuration has been simulated in the second case study. The downstream turbine has suffered an extremely high power loss of 86%. This is attributed to the absence of atmospheric turbulence, which would catalyze the breakdown of vortices existing in the incoming wake. Hence, power loss has been over-estimated by a large amount.

It is concluded that the Actuator Line Model is a promising and relatively inexpensive method in capturing wake interactions, especially in simulations with numerous rotors and large field dimensions, but requires accurate selection of simulation parameters and it is sensitive to the atmospheric conditions.

References

- Bachant, Pete (2016), *Actuator line modeling extension library for OpenFOAM*, <https://github.com/turbinesFoam/turbinesFoam>, 2002
- Bianchi, Fernando and De Battista, Hernán and Mantz, Ricardo Julian (2007), *Wind Turbine Control Systems: Principles, Modelling and Gain Scheduling Design*
- Burmester, S. and Gueydon, S. and Make, M. (2016), *Determination of scaled wind turbine rotor characteristics from three dimensional RANS calculations*, Journal of Physics: Conference Series, vol. 753, 09 2016.
- Dose, B. and Rahimi, H. and Herráez, I. and Stoevesandt, B. and Peinke J. (2018), *Fluid-structure coupled computations of the nrel 5 mw wind turbine by means of cfd*, Renewable Energy, vol. 129, 05 2018

- Drela, Mark (1988), *XFOIL: Subsonic Airfoil Development System*, <http://web.mit.edu/drela/Public/web/xfoil/>, 1988
- Jonkman, J. and Butterfield, S. and Musial, W. and Scott, G., *Definition of a 5-mw reference wind turbine for offshore system development*, Tech. Rep. NREL/TP-500-38060, National Renewable Energy Laboratory, 2009.
- Marten, D. and Wendler, J. and Pechlivanoglou, G. and Nayeri, C.N. and Paschereit, C.O. (2013), *Qblade an open source tool for design and simulation of horizontal and vertical axis wind turbines*, IJETAE 3 special issue pp. 264–269 2013, 2013.
- Schmitz, S. and Jha, P. (2013), *Modeling the wakes of wind turbines and rotorcraft using the actuator-line method in an openfoam -les solver*,
- Shen, W. Z. and Mikkelsen, R. and Sørensen, J. N. and Bak, C. (2005), *Tip loss corrections for wind turbine computations*, Wind Energy, vol. 8, no. 4, pp. 457–475, 2005
- Smagorinsky, J. (1963), *General circulation experiments with the primitive equations*, Mon. Weather Rev., vol. 91, 01 1963.
- Sorensen, Jens Norkaer and Shen, Wen Zhong (2002), *Numerical Modeling of Wind Turbine Wakes*, Journal of Fluids Engineering 124, 2002
- Weller, H.G. and Tabor, G. and Jasak, H. and Fureby, C. (1998), *A tensorial approach to computational continuum mechanics using object-oriented techniques*, COMPUTERS IN PHYSICS, VOL. 12, NO. 6, NOV/DEC 1998.